Surveys in Geophysics manuscript No.
(will be inserted by the editor)

New advances in the knowledge of the structure of Tenerife volcanic island derived from seismic attenuation tomography

J. Prudencio · J. M. Ibáñez · E. Del Pezzo · J. Martí · A. García-Yeguas · L. De Siena

Received: date / Accepted: date

J. Prudencio
Earthquake Research Institute, University of Tokyo, 1-1 Yayoi, Bunkyo-ku, 113-0032 Tokyo, Japan
Instituto Andaluz de Geofísica, University of Granada, Profesor Clavera 12, 18071 Granada, Spain
E-mail: janire@ugr.es

J. M. Ibáñez
Instituto Andaluz de Geofísica, University of Granada, Profesor Clavera 12, 18071 Granada, Spain
Dept. Fisica Teórica y del Cosmos, University of Granada, Fuentenueva S/N, 18001 Granada, Spain
Istituto Nazionale di Geofisica e Vulcanologia, Sezione di Catania -Osservatorio Etneo, 95125 Catania, Italy

E. Del Pezzo
Istituto Nazionale di Geofisica e Vulcanologia, Sezione di Napoli -Osservatorio Vesuviano, Via Diocleziano 328, 80124 Naples, Italy
Instituto Andaluz de Geofísica, University of Granada, Profesor Clavera 12, 18071 Granada, Spain

J. Martí
Instituto de Ciencias de la Tierra Jaume Almera, CSIC, Lluis Solé Sabaris S/N, 08028 Barcelona, Spain

A. García-Yeguas
Dept. Física Aplicada, University of Cádiz, Av. Duque de Nájera 18, 11002, Cádiz, Spain
Instituto Andaluz de Geofísica, University of Granada, Profesor Clavera 12, 18071 Granada, Spain
INVOLCAN, Antiguo Hotel Taoro, Parque Taoro 22, 38400 Puerto de la Cruz, Tenerife, Spain

L. De Siena
University of Aberdeen, School of Geosciences, Geology and Petroleum Geology, Meston Building, King's College,AB24 3UE Aberdeeen, Scotland

Abstract This manuscript shows a new multidisciplinary interpretation approach of the internal structure of Tenerife island. The cental core of this work is the determination of the three dimensional attenuation structure of the region using P-waves and the Coda Normalization (CN) method. This study has been performed using 45303 seismograms recorded in 85 seismic stations from an active experiment (air-gun shots) conducted in January of 2007. The interpretation of these new results is done combining the new images with previous studies performed in the area such as seismic velocity tomography, magnetic structure, magnetotelluric surveys or gravimetric models. Our new 3D images indicate the presence of seismic attenuation contrasts, with areas of high and low seismic attenuation patterns. High seismic attenuation zones are observed both in shallow and deeper areas. The shallowest area of Las Cañadas Caldera complex (1-3 km thick) is dominated by high attenuation behavior and it is interpreted as the combined effect of sedimentary and volcanoclastic deposits, multifracturated systems and the presence of shallow aquifers. At the same time, the deeper analyzed area, beyond 8 km below sea level, is dominated by high attenuation pattern and it is interpreted as the consequence of the effect of high temperature rocks in the crustal-mantle boundary. This interpretation is compatible and confirmed by previous models that indicate the presence of underplating magma in this region. On the contrary, some low attenuation bodies and structures have been identified at different depths. A deep low attenuation central body is interpreted as the original central structure associated to the early stage of Tenerife island. At shallower depths, some low attenuation bodies are compatible with old intermediate magmatic chambers postulated by petrological studies. Finally, in the North of the island (La Orotava valley) we can interpreted the low attenuation structure as the headwall of this valley supporting the idea that Las Cañadas Caldera and this valley resulted from two different destructive processes. This first 3D attenuation structure is an important evidence that seismic attenuation tomography studies are essential to better understand the structure of volcanoes and will allow us to better identify the main constraints on the dynamics of active volcanoes.

Keywords Attenuation · Scattering · Tomography · Tenerife · Canary Islands

1 Introduction

Obtaining comprehensive models on the dynamics of volcanic systems, combining geological and geophysical data, is important to understand their past behavior and to predict their future activity. Different high precision geophysical techniques, such as seismic tomography, magnetotelluric or gravimetry, provide good insights on the internal structure of volcanic systems, and when combined with stratigraphic, structural, petrological and geochemical data, may allow us to identify the main constraints on the dynamics of a particular volcano. Recently, seismological studies of volcanic regions are introducing a new and stable tool to add new and valuable information of the internal structure: seismic attenuation tomography. This technique is based in the study in heterogeneous media of the dissipation and scattering of the seismic waves (Del Pezzo 2008). The advantage of this procedure in comparison to the classical velocity tomography is that seismic wave attenuation is more sensible to the physical contrast of the medium (Sato et al 2012). In the last years many examples highlight this evidence. Thus, Martínez-Arevalo et al (2005) in their study of Etna volcano confirmed the presence of a high consolidate body in the central structure of the volcano that modifies the magma path in its ascent producing new adjacent vents. In a similar way, Del Pezzo et al (2006) and De Siena et al (2010) studied Vesuvius and Campi Flegrei volcanic regions, respectively, using attenuation properties. These authors confirmed the high contrast of attenuation associated to unconsolidated, high consolidate, hydrothermal systems and partial melt materials in both neighboring volcanic regions. In Mount St. Helens volcano De Siena et al (2013) used different attenuation techniques identifying important volcanic structures such as the main path of magma ascent from depth. In other sense, Prudencio et al (2015) confirmed the effects of unconsolidated materials, hydrothermal system and partial melt rocks under Deception Island in the pattern of attenuation. In addition, in the same volcano, the contrast of the cristaline basement and volcanic structure observed by Zandomeneghi et al (2009) is more clearly detected when separation of intrinsic and scattering attenuation is obtained (Prudencio et al 2013b). These observations done in Deception volcano caldera are very close to other performed in a very similar volcano, but located in an opposite region (Alaska against Antarctica), as those made in Okmok volcano (Ohlendorf et al 2014). As De Siena et al (2013) concluded: ”these techniques represent the future of seismic volcano imaging”.

Tenerife island is the largest, highest and the most complex island of Canary archipelago (Spain). In terms of its historical eruptions records at least seven eruptions have been reported (Romero-Ruiz 1991) in the last 500 years. The Holocene eruptive record includes several tens of monogenetic eruptions and at least 16 eruptions from the central complex Teide-Pico Viejo (Carracedo et al 2007; García et al 2014). The scientific importance of this island is evidenced by the large number of geological, geophysical and geochemical studies performed on it in the last decades. Despite, of this large number of studies, at the present there is a non unique model of the evolution of the island and neither of its internal structure, and even the origin of the whole archipelago is still a close topic and few theories could be considered at the present as potentially valid (e.g. Fullea et al 2015).

In the present work we perform a seismic attenuation tomography of Tenerife Island using P-waves and the Coda Normalization method (De Siena et al 2014). Data used in this study were obtained by an active seismic experiment performed in 2007 (Ibáñez et al 2008) and were used to obtain a high resolution velocity tomography of the same region (García-Yeguas et al 2012). The objective of this paper is to provide new information on the inner structure of the island that could permit to better understand the volcanic framework of the region. This information will be interpreted jointly with other geological and geophysical evidences and will allow us to propose an advanced model of the internal structure of the island. Since results of seismic attenuation are robust and reliable we are certain that this new interpretation will help significantly in the improvement of the knowledge of the region.

2 Geological and Geophysical framework

2.1 Geological introduction

Tenerife is the largest (2058 km^2) and highest (3718 m) island of the Canarian archipelago (figure 1). The geological evolution of Tenerife involves the construction of two main volcanic complexes: a basaltic shield complex (>12 Ma-to present, Abdel-Monen et al 1972; Ancochea et al 1990; Thrilwall et al 2000); and, a central complex (< 4 Ma to present, Fúster et al 1968; Araña 1971; Ancochea et al 1990; Martí et al 1994). The basaltic shield complex is mostly submerged and forms about the 90% of the volume of the island, continuing at present its subaerial construction through two rift zones (Santiago Rift Zone and Dorsal Rift Zone, figure 1). The central complex comprises the Cañadas edifice (< 4 Ma-018 Ma), a composite volcano characterized by several explosive eruptions of highly evolved phonolitic magmas, and the active Teide-Pico Viejo twin stratovolcanoes (0.18 ka to present) (figure 1). These last have evolved from basaltic to phonolitic and have mostly undergone effusive and explosive activity. The Cañadas caldera, in which the Teide-Pico Viejo stratovolcanoes stand, truncated the Cañadas edifice and was transformed by several vertical collapses, which were occasionally associated with lateral collapses of the volcano flanks (Martí et al 1994; Martí et al 1997; Martí and Gudmundsson 2000).

Recent volcanic activity is mostly represented by monogenetic basaltic volcanism located along the rift zones or scattered throughout the southern part of the island (Southern Volcanic Zone, figure 1) and, by the Teide-Pico Viejo stratovolcanoes (figure 1), with basaltic to phonolitic emissions (Martí et al 2008).

The evolution of subaerial volcanism on Tenerife has been controlled mainly by the ENE-WSW and NW-SE oriented tectonic trends (Martí et al 1996). Evidence comes from geophysical studies of the oceanic basement around and below the Canary Islands (Dash and Bosshard 1969; Bosshard and MacFarlane 1970; Verhoef et al 1991; Mezcua et al 1992; Roest et al 1992; Watts et al 1997; Mantovani et al 2007) and from dikes distribution and the alignments of recent mafic vents. The predominance of these tectonic trends on Tenerife during its whole history suggests the importance of a long-lived regional tectonic control on the ascent of mantle-derived magmas and the distribution of volcanism.

Morphologically, the island of Tenerife is characterized by the superposition of the two volcanic complexes, basaltic shield and Las Cañadas edifice, which confer the characteristic pyramidal profile to the island. However, it is also important to mention the existence of four large depressions formed during destructive episodes and that correspond to the Las Cañadas caldera at the central part of the island and to the landslides valleys of Guimar, to the south, and La Orotava and Icod to the north (figure 1).

As indicated above, Tenerife has been the focus of several volcanological, geological, geochemical and geophysical studies in recent years. In the bibliography there are recent works that provide a complete and well structured review of them, such as: Soler-Javaloyes and Carracedo (2013), Piña-Varas et al (2014) or García et al (2014).

In the present review we will focus our description on those works that will help us to better understand and interpret our results, which basically are works on magnetic properties, magnetotellurics and seismic tomography.

2.2 Magnetic properties:

Recently, Blanco-Montenegro et al (2011) presented a 3D structural model of Tenerife island based on high-resolution aeromagnetic data. These authors identify a central basaltic shield that they interpreted as the origin of the island. This structure support the model of an unique origin of the island in opposition to the three-armed rift system that could be present in the early stage of the island. Additionally, they identified the existence of consolidated dikes surrounding this central shield, interpreted as the consequence of magma intrusion from the early volcanic phases of the island. Additionally, in the shallower part of the island they identify some geometries that can be interpreted as round local landslides. Finally, they support the idea that the origin of the Las Cañadas caldera is associated with a vertical caldera collapse.

2.3 Magnetotelluric properties:

Pous et al (2002) in their magnetotelluric study of Las Cañadas caldera found an area with high conductive anomaly that was interpreted by the existence of high fractured rocks and fossil hydrothermal alteration located parallel and close to caldera wall marking the position of the structural border of the caldera. Additionally, they identified two main shallow aquifer zones in this area. This results support the theory of multiple vertical collapse origin of the area. Similar results were observed by Coppo et al (2008) using a more complete audio-magnetotelluric sounding profiles. They confirmed that Las Cañadas caldera structure is the result of at least 3 vertical collapse of different volcanic edifices occurred during the last million year. Piña-Varas et al (2014) studied the resistivity structure of Tenerife using different magnetotelluric surveys. They observed several areas with low resistivity values that mainly are associated to the presence of many geothermal systems. They performed a preliminary correlationship with P-wave velocity models that also is the topic of the already unpublished paper (García-Yeguas et al. 2015, in preparation). These authors found a deep area of medium resistivity values that are interpreted as potential partial melt region that could be the energy source of the hydrothermal activity.

2.4 Seismic tomography and seismic studies:

García-Yeguas et al (2012) presented the first seismic tomography image of Tenerife island using active seismic data obtained in the TOM-TEIDEVS experiment (figure 2) carried out in January 2007 (Ibáñez et al 2008). The inversion of this data permits to obtain a 3D velocity model from the top of the island (Teide-Pico Viejo-Cañadas Complex) to 8-10 km bellow sea level. One of the main conclusion of this work is the presence of an unique high velocity structure at the maximum resolve depths in the center of the island. This central structure characterized by high P wave velocity was interpreted in concordance with other observations and hypothesis done for example by Martí et al (1994), Ablay and Kearey (2000), Pous et al (2002), Gottsmann et al (2008) or Geyer and Martí (2010) that postulate the presence of a single basaltic shield and therefore, the formation of Tenerife arising from a single central volcanic structure. This interpretation is in agreement with Blanco-Montenegro et al (2011). The surrounding and shallower regions are characterized by low velocity structures which are associated to unconsolidated materials, hydrothermal alterations and the residual effects of recent volcanic eruptions. Prudencio et al (2013a) obtained 2D regional distribution of seismic attenuation separating scattering and intrinsic contribution (Q_i^{-1} and Q_s^{-1}, respectively). As their main results, we can mention the existence of a region in the middle of Tenerife Island with low attenuation interpreted as the effect of intermediate/deep consolidate rocks. Surrounding this central body, there are several areas dominated by high attenuation effects. These external areas, also characterized by low P-wave velocity, were interpreted as complex fractured regions, hydrothermal alteration and the presence of volcanoclastic deposits, among others. In the whole island scattering phenomena is more important (in terms of attenuation contribution) than intrinsic attenuation. De Barros et al (2012) analyzed the potential effects on secondary arrivals produced by possible structures that generate scattered waves. They used the same data set of García-Yeguas et al (2012) and they identified two main bodies, one located at 7-9 km b.s.l. in the north part of the island and other at 1-4km b.s.l. below the Cañadas Caldera. They associate this shallow structure to a potential phonolitic storage area that could feed the Teide-Pico Viejo complex in the past. The presence of important structures that produce coherent scattered waves in Tenerife was already observed, also at shallow regions, by Del Pezzo et al (1997). At deeper zones Lodge et al (2012) studied received functions recorded with the same seismic stations that above authors. They found magmatic underplating beneath Tenerife island and areas of low velocity that are interpreted as partial melt regions at depth below 8-10 km b.s.l. These observations are in agreement with a previous study of Dañobeitia and

Canales (2000). These authors found two regions of low velocity below the main volcanic edifice. The shallower one located around 4-8 km b.s.l. and the deeper one, characterized by low crustal P-wave velocity and located near the crustal-mantel boundary. They located this area between 17 to 25 km b.s.l. and it is interpreted as a magma underplating below Tenerife island. The natural seismicity of the island at the present is very low (Almendros et al 2000, 2007) and also due to the reduce number of permanent seismic stations in the island, seismic source models are not too accurate. Recently, Domínguez Cerdeña et al (2011) relocated the seismic activity associated to a strong seismic swarm occurred during 2004-2005. These authors proposed a source-model of this seismic swarm in which a possible magma intrusion at depth around 4 km (b.s.l.) takes place in the central part of the island below Teide volcano. The seismicity is the brittle response of the medium due to the effect of the increase of the pressure due to magma and gases movement. This magma intrusion was not observed neither with the magnetic inversion nor the seismic velocity tomography.

3 Data and method

3.1 Data

In this study we used initially the dataset used to obtain 3D velocity structure by García-Yeguas et al (2012) composed by 103,750 waveforms. In Figure 3 we show four recordings produced by a shots located in the north and registered at stations 14, 75, 40 and 51 of TOM-TEIDEVS experiment. These stations are located either on or around Teide volcano. The corresponding waveforms show good signal-to-noise ratio after filtering data in the 4-8 frequency band (central frequency 6 Hz). This frequency band was chosen as it provides stable and reliable results for the separate images of intrinsic and scattering attenuation as shown by Prudencio et al (2013a). The final data-set is comprised of 45303 vertical seismic waveforms. The waveforms were selected depending on the signal-to-noise and coda-to-noise ratios (always larger than 2) at 6 Hz.

3.2 Velocity model and ray tracing

García-Yeguas et al (2012) used the waveform-dataset produced by the TOM-TEIDEVS active seismic experiment Ibáñez et al (2008) to invert 3D distribution of absolute P-wave velocities under the island. P-wave travel-times are inverted using the code ATOM-3D, a tomography algorithm adapted by Koulakov (2009) for the 3D tomographic inversion based on active seismic data. The velocity model is distributed on a set of nodes whose distance depends on ray density and spans an area of 40x40 km^2. The minimum node spacing is set at 0.7 km and a continuous velocity distribution, necessary for the application of the ray-tracing, is obtained by linear interpolation.

On this velocity model, we used the Thurber-modified ray-bending approach described, e.g., by De Siena et al (2010). The vertical ray distribution is plotted in Figure 2. This ray-tracing algorithm has recently been tested and applied to active waveform data by Prudencio et al (2015) at Deception Island. Between surface and a depth of 12 km a count of ray density confirms the applicability of attenuation tomography between depths of -2.2 and 12 km. Therefore, the velocity and attenuation models are comparable if we use a grid having the same lateral extension of the first grid described by García-Yeguas et al (2012).

3.3 *P*-wave attenuation tomography with the coda normalization method

The coda-normalization (CN) method provides attenuation measurements in a given frequency band with central frequency f_c by calculating the ratio between the measured direct-P or -S energy (E_k^s) and coda-P or -S energy in a time window centered around a given lapse time t_c ($E_k^c(f_c, t_c)$). The single-path CN equation is:

$$\frac{1}{\pi f_c} ln(\frac{E_k^s(f_c)}{E_k^c(f_c, t_c)}) = K(f_c, t_c, \theta, \phi) - \frac{2}{\pi f_c} \gamma ln(r_k) - 2 \int_{r_k} \frac{dl}{v(l)Q(l)} \quad (1)$$

where r_k is the total length of the k^{th} ray, γ is the geometrical spreading, that we invert tighter with the attenuation parameters (La Rocca et al 2001; Morozov 2011; De Siena et al 2014) and $v(l)$ is the velocity of the medium measured along the ray-path. $K(f_c, t_c, \theta, \phi)$ correspond to the effect of the source radiation pattern, described by the take-off angle (θ) and azimuth (ϕ) and is the only other unknown variable (apart for Q) in the equation.

As shown by Yoshimoto et al (1993) we can extend the CN method to the measurement of *P*-wave average attenuation (the *P*-wave quality factor, Q_p) by using passive seismicity. Prudencio et al (2015) applied the method to an active seismic dataset similar to that used in this study.

We invert the P-to-coda energy ratios with the MURAT code in a single-step inversion (De Siena et al 2014). We set the start-time of the coda time-window duration 3 s to a lapse-time of 17 s. The P-energy time window is set to 1.5 s. The inversion of the energy ratios for the average parameters provides an average Q_p of 125. In the following, we represent the variations with respect to the inverse of the average quality factor in the 3D space (ΔQ_p^{-1}, in %).

4 Resolution, stability and robustness tests

In order to check both robustness of the algorithm and the reliability, stability and resolution of the results we perform (1) a checkerboard test, (2) a jack-knifing test, (3) a test of the influence of the velocity model on results and (4) a synthetic anomaly test mimicking the results.

4.1 Checkerboard test

In order to test the resolution of the entire region we performed the well-known checkerboard test, whose results are shown in Fig. 4 (horizontal slices) and Fig. 5 (vertical sections). We generated synthetic P-to-coda energy ratios and we added Gaussian random error with zero mean and 3 times the standard deviation, equal to the 20% of the data value. We inverted the synthetic data using blocks crossed by at least 10 rays with 2.8 km node spacing, starting at 2.2 km, and having quality factors equals to 100 or 1000. The checkerboard test results are well resolved in all obtained depths. In the horizontal slices, some external regions below 6.2 km (b.s.l.) have a limited resolution that will not affect to our final interpretation.

4.2 Jackknifing test

To test the robustness of the data, we applied a jackknife test consisting on the random removal of different percentage of data. The results of the test are shown in Fig. 6a,b,c. As can be observed, the main attenuation patterns does not change up to a 40% removal of the data. The large number of event used gives us a strong stability of our final images that will be unaffected by potential lack of data.

4.3 Influence of velocity model

In order to check the influence of the velocity model on our attenuation results, we proceeded to randomly disturb it using some amount of noise. The procedure was to introduce some percent of random variation in the 3D velocity model and to check the potential variations of the 3D attenuation model. The not perturbed model is shown in figure 6d. We tested with 5 and 10% of Gaussian noise and the obtained attenuation images (Figure 6e,f) are almost identical to the original. This result demonstrate that our attenuation model is not coupled (no trade-off) with the velocity model and the observed stability could be again associated to the large number of used data.

4.4 Synthetic anomaly test

We also tested the resolution of our results by assuming different synthetic anomalies of high and low attenuation and different size. We imposed:10x20x6 km^3 very low attenuation anomaly in the north coast, 10x10x5 km^3 low attenuation anomaly in the southwestern region, 20x15x8 km^3 high attenuation anomaly in the northwestern zone and 5x5x5 km^3 very high attenuation anomaly in the central part of Tenerife island. We add the same amount of Gaussian random error to the synthetic P-to-coda energy ratios calculated from the checkerboard test and inverted the synthetic data. The obtained results are shown in Fig. 6g,h,i. All the anomalies are well reproduced which points out the good resolution of the region under study. The high density of rays provides us a good tool to solve with quality and confident the area under study.

5 Results and Discussion

The association of seismic attenuation anomalies to the corresponding rock properties is at the present a complex task. Nowadays, the geological interpretation of the tomographic images is mostly based in physical interpolations and qualitative considerations, even if laboratory experiments and measurements are providing new evidences among their relationship. Vanorio et al (2005) report a detailed discussion about the rock physics parameters and their relationship with seismic velocities at Campi Flegrei Caldera (Southern Italy), giving insights into the dependence of V_p and V_s velocity from pore fluid pressure, porosity and temperature. More difficult is the interpretation of the attenuation anomalies. Total-Q (the parameter which is generally represented in attenuation tomography) is the combination of intrinsic-Q and scattering-Q. The separate estimate of these two parameters is needed for a correct discrimination between temperature effects (lowering intrinsic-Q, see De Lorenzo et al 2001) and the contribution of strong heterogeneities (lowering scattering-Q, see Sato et al 2012). Moreover, the S-wave and P-wave attenuate in a different way in the same rock typology. V_p is relatively unaffected by the presence of fluid elements in the rock matrix, while a strong decrease of V_s velocity should be presented. Intrinsic-Q for P-waves should result relatively poorly changed, while a strong decrease in both P- and S-waves scattering-Q should be presented. We have reported some examples of possible interpretations in table 1, which can be useful when multiple images based on different seismic attribute measurements are jointly available in the same region.

5.1 Tenerife Island Q values

The inversion of the energy ratios for the average parameters provides an average Q_p of 125. In general this average Q value is low in comparison to the expected average Q value for the Earth's crust (Sato et al 2012). According to the resolution test performed in section 4, the optimum size of the grid inversion is the use of cells of dimension of $2.8x2.8x2.8$ km. In figure 7 we plot the five horizontal slices obtained from 2.2 km (above sea level) to the maximum depth of 9 km (below sea level). In figures 8 and 9 we show six vertical sections: 3 S-N direction and 3 in the W-E direction as indicated in figure 4b. Observing these figures we can identify the following main characteristics:

1. At shallower depths (over 5-6 km b.s.l.) Tenerife Island is mainly characterized by a low seismic attenuation structure (the general green color

observed in figures 8 and 9). This observation is mostly common in several volcanic areas studied such as Mt. Vesuvius (De Siena et al 2009, Tramelli et al 2009), Campi Flegrei (De Siena et al 2010) or Etna volcano (Martínez-Arevalo et al 2005, Alparone et al 2012). In general, this low attenuation, that also is coincident with the high velocity structure, is interpreted as the response of consolidate and cold materials, as expected of classical stratovolcanoes.

2. At larger depths (underneath 6 km b.s.l.) high seismic attenuation dominates in the hole region (orange and red color in the bottom of figures 8). The observed low Q values can be associated to the potential presence of warmer materials with plastic behavior. Previous studies (e.g. Watts et al 1997; Dañobeitia and Canales 2000; Lodge et al 2012) have identified the possible existence of magma underpplating beneath Tenerife Island analyzing seismic and other geophysical evidences. These authors identified the Moho below Tenerife at a depth around 15-18 km locating the magma underplating around or upon the Moho. In these studies, several discontinuities are observed such as, crust-sediment or sediment-volcanic edifice. These zones are optimal for magma accumulation. This evidence is also confirmed with petrological analysis of mafic rocks which show differentiation characteristics (Ablay 1997, Neumann et al 1999, Thrilwall et al 2000).
3. At very shallow depths (close to the surface) we can identify few areas with high seismic attenuation (e.g. H1 anomaly of figures 7 and 8). This anomaly is located just in the Las Cañadas caldera edifice. According with geophysical studies of Coppo et al (2008), Coppo et al (2010), Piña-Varas et al (2014) and Villasante-Marcos et al (2014) the caldera is filled by unconsolidated rocks and highly fractured material from Teide-Pico Viejo stratovolcanoes. Additionally, they identified in the caldera the presence of hydrothermally altered rocks and shallow aquifers. It is remarkable that H1 anomaly has a very similar geometry of these complex and altered structure. However, the resolution used in figure 8 can not allow us to observe additional details. It is also worth mentioning that the contrast in seismic attenuation values surrounding the H1 anomaly, could be identified as the limit of the caldera depression. Similar observations of the effect of shallow unconsolidated material has been done in Deception Island (Prudencio et al 2015), Okmok volcano (Ohlendorf et al 2014) or Campi Flegrei (De Siena et al 2010).
4. A remarkable result is the identification in the inner of Tenerife island of several structures characterized by very low attenuation, L1, L2 and L3 of figures 7, 8 and 9. These low attenuation structures are usually identified as consolidate cold magmatic bodies, e.g. Etna (Martínez-Arevalo et al 2005), Vesuvius (Tramelli et al 2009). These rigid bodies additionally can act as reflecting or scattering structures. These structures can affect the composition of the coda waves of local seismograms, as observed by Del Pezzo et al (1997) or can be identified as strong coherent arrivals in the coda of the used signal and draw the position of them as performed

by De Barros et al (2012). It is remarkable that anomalies L1, L2 and L3 were previously identified by the above authors using scattered seismic waves (figure 8 from De Barros et al (2012)). These authors interpreted these bodies as possible ancient magmatic chambers that fed eruptions of the last 2000 years occurred in Teide-Pico Viejo-Las Cañadas Complex. In fact, these anomalous bodies could correspond to crystallized magma emplace at the main rheological discontinuities that exist inside Tenerife, these being the base of the volcanic edifice (at 4-5 km b.s.l), the contact between Miocene sediments and the basaltic oceanic crust (5-7 km b.s.l) and the crust/mantle boundary (15-16 km b.s.l). The existence of magmatic reservoirs or underplating at such depths during certain stages in the evolution of Tenerife is also evidenced by the existing seismic reflection profiles (Watts et al 1997; Dañobeitia and Canales 2000) and petrological data (Ablay 1997; Neumann et al 1999; Thrilwall et al 2000), which suggest that mafic magmas appearing on Tenerife have occasionally been evolving at such depths or equivalent pressures.

5. Outside of Las Cañadas Caldera we identify low attenuation area marked in figures 7, 8 and 9 as L4 anomaly. This anomaly can not be linked directly to the other structures. It is located in the North of Tenerife Island in a region called Orotava Valley (figure 1). This shallow low seismic attenuation zone can be interpreted as resulting from the high contrast exerted by the basaltic shield in a zone where the Cañadas edifice succession was removed by the formation of the landslide valley. This valley was subsequently infilled. This also suggest that the headwall of this valley does not affect the interior of the Cañadas caldera, thus supporting the idea that the caldera and the Icod valley resulted from two different destructive processes (see Martí et al 1997).
6. There is an interesting high attenuation area located at intermediate depths (H2 in figure 7 and 8) and could be associated to recent eruptions. This zone located below a region in which a strong fissural eruption took place at the beginning of the XVIII century (1704-05 Fasnia-Arafo-Siete Fuente eruptions, see figure 1) (Romero-Ruiz 1991). Making a vertical profile in figure 8d, on the top of H2 we identify a shallow high attenuation area that can be interpreted as the effect of volcanoclastic deposits of the eruptive processes. Between the surface and H2 the lower attenuation zone can be associated to cooled conduits, and H2 is the effect of the remain hot materials at depth. This area is characterized also by low P-velocity. We can interpret the observed values as the effect of volcanoclastic deposits in surface combined with the remain hot materials in depth.

5.2 Velocity vs. attenuation

It is observed that P-wave velocity and attenuation images match each-other at shallow depths (from surface till to 4-5 km depth). In this depth range the coincidence between high velocity and low attenuation zones predominates. The predominance of high-attenuation correspondent to low velocity at surface is generally interpretable as due to the presence of partially unconsolidated materials, with possible presence of water layers. A complete different pattern can be observed at higher depths, where the high attenuation zone does not correspond to a low velocity zone. This is possibly due to lack of resolution effects which could be present in the deepest borders of the volumes investigated with the velocity tomography, which unfortunately coincide with the zone with high attenuation. On the other hand, the high attenuation zone present at 6 - 10 km everywhere below Tenerife, is well inside the optimal resolution achievable with the attenuation tomography technique utilized in the present paper.

5.3 Las Cañadas-Teide-Pico Viejo Complex attenuation structure

As indicated above, the cells size used for the inversion cannot permit to solve with enough details some structures. However the ray coverage shown in figure 2 suggests that the center of the island could be inverted with higher resolution. It is remarkable that this region is coincident with Las Cañadas-Teide-Pico Viejo complex. Around Teide volcano there is a region of 10x10 km in which cells of 1.4x1.4x1.4 km have optimal resolution (figure 10) up to a depth of 6 km b.s.l. Vertical attenuation profiles (N-S and W-E) are plotted in figure 10. The new images show that the maximum thickness of the collapsed zones, represented by the high attenuation H1 anomaly, of Las Cañadas Caldera is between 1.5 and 2 km, coinciding with new structural estimates for the collapse of this caldera (Iribarren 2014). Other remarkable new results are the identification of two new small low attenuation bodies located just bellow the Teide-Pico Viejo volcanic complex (L5 and L6 in figure 10). They can be interpreted as old potential shallow magma reservoirs. The existence of these small ancient magma bodies have been frequently assumed to be located in this zone. When the Cañadas edifice was active this zone accumulated most of the intrusions of deeper mafic magma in the central part the island due to the shadow effected that phonolitic chambers exerted on more deeper magma avoiding them to reach the surface at that zone (Martí and Gudmundsson 2000). In consequence, most of mafic magmas intruding below the shallow phonolitic systems crystallized there forming dense bodies of gabros, as it is testified by high gravimetric positive anomalies (Ablay and Kearey 2000; Gottsmann et al 2008) and the present of gabroid xenoliths in some Las Cañadas caldera forming pyroclastic deposits (Martí et al 1994; Pittari et al 2008). The same area seems to be the site today for the accumulation of deeper magmas that then differentiate and evolve into the phonolites that feed Teide-Pico Viejo eruptions, as it is indicated by experimental petrology data (Andújar et al 2010). Therefore, such small phonolitic reservoirs, assumed from the size of the last phonolitic eruptions (see Martí et al 2008) have been able to be identified with the present higher resolution.

6 Conclusions

In the present work we provide new observations and interpretations of the inner structure of the volcanic island of Tenerife on the base of the first high quality 3D attenuation tomography. The seismic attenuation images are combined with previous geophysical, petrological and geological observations providing an integrated vision of the zone.

In general the whole region is dominated by low attenuation structures, as expected for a volcanic environment. A first regional inversion with lower resolution allowed as to clearly associate the deeper high attenuation anomalies with the potential magma underplating predicted previously by several authors. The central zone of the island, characterized by a single low attenuation structure, is an additional evidence that could support the theory that Tenerife island evolved in its origin from a potential single source rather than a possible three arms structure. In this rigid structure, lowest attenuation anomalies are associated to intermediate-deep ancient magmatic chambers that could feed the volcanic complex. At the surface the island has strong attenuation contrasts. In some areas high attenuation anomalies are evidenced, such as Las Cañadas edifice or the regions in which recent historical eruptions occurred. These high attenuation behavior is interpreted as the combined effect of volcanoclastic deposits, sediments, multifracture structures, hydrothermal alterations or shallow aquifers. The shallow low attenuation body located in La Orotava valley could provide additional evidences that the destructive processes associated to this valley and Las Cañadas edifices could be originated independently.

A higher resolution images performed around Teide volcano permitted to better constrain the depth and size of the infilled Cañadas caldera and to identified a few cooled structures that could be associated to ancient shallow phonolitic reservoirs.

As a final conclusion, we can infer that the attenuation studies are a fundamental tool to better constrain the physical properties of volcanic regions and therefore, contribute with solid arguments that could help to better understand the volcano dynamics.

7 Table captions

Table 1:Different values of P- and S-wave velocity and attenuation parameters and Vp/Vs ratio and its possible interpretation based on scientific papers reporting such interpretations.

8 Figure captions

Fig. 1: Regional setting and location of Tenerife Island in the Canary Islands archipelago (Spain). White triangle correspond to the position of Teide

volcano, white lines correspond to rift position and Las Cañadas wall is also marked with white line. IV Icod Valley, OV Orotava Valley, SRZ Santiago Rift Zone, DRZ Dorsal Rift Zone, PV Pico Viejo, LCC Las Cañadas Complex, GV Guimar Valley, FASF Fasnia-Arafo-Siete Fuentes eruption and SVZ South Volcanic Zone (modified from Fig. 1 of Martí et al (2012)). We marked the higher resolution area of figure 10.

Fig. 2: Configuration of TOM-TEIDEVS seismic tomography experiment. Stations are represented with red triangles and shots locations with gray dots. 3D source-station ray-paths obtained by using Thurber-modified ray-bending approach are represented below.

Fig. 3: Four examples of vertical records of a seismic shot produced on the 19 of January 2007 located in the north of Tenerife (gray star) and recorded at four onland seismic stations 14, 75, 40 and 51 (gray squares). P-window and Coda-window lengths used in the analysis are represented with blue and red squares, respectively. The panels on the bottom show the P-wave (blue line), Coda (green line) and Noise (red line) spectra for each seismogram. We marked the frequency band analyzed in the present work by dashed line.

Fig. 4:The input (top left) and output of the checkerboard test are shown on five horizontal slices taken at different depths (2.2 km a.s.l and 0.6, 3.4, 6.2 and 9 km b.s.l.). Tenerife Island contour is over-imposed on each panel. In the 2.2 km a.s.l. panel (top right) the position of the vertical sections of next figures are shown.

Fig. 5:The input and output of the checkerboard test are shown for six vertical sections, three in S-N direction and three in W-E direction (see figure 4). The vertical scale is enlarged for clarify.

Fig. 6: Different stability and robustness tests are shown: Jackknifing test images with 100% of the data (a), 80% of the data (b) and 60% of the data (c); velocity model influence test with no noise added (d), with +5% of Gaussian noise (e) and with +10% of Gaussian noise (f) and synthetic anomaly test input (g) and two horizontal slices through the output of the test at 0.6 and 3.4 km b.s.l. (h,i).

Fig. 7: The results of the attenuation tomography are shown for the five horizontal slices taken at different depths: a) +2.2 km, b) -0.6 km, c) -3.4 km, d) -6.2 km and d) -9 km. The color scale show the variations (in percent) of the attenuation model with respect to the average quality factor. The high and low attenuation anomalies discussed in the text are shown as white squares and with white labels (H1, H2, L1, L2, L3, L4).

Fig. 8: The results of the attenuation tomography model are shown in six vertical sections crossing the island (see figure 4): a) SN 1, b) WE 1, c) SN 2, d) WE 2, e) SN 3 and f) WE 3. The color scale show the variations (in percent) of the attenuation model with respect to the average quality factor. The high and low attenuation anomalies discussed in the text are shown as red squares and with red labels (H1, L1, L2, L3, L4).

Fig. 9: 3D perspective view of the final attenuation tomography model.

Fig. 10: 3D perspective view of the final attenuation tomography model. High-resolution results of the attenuation tomography model are shown for

Las Cañadas area (see figure 1) in two vertical sections (SN and WE). (0,0) coordinates correspond to the position of Teide volcano, same as for SN 2 and WE 2 profiles in figure 8c and 8d but for a smaller area of 10x10 km^2. Top panels (a,b) are the output of the checkerboard test. Bottom panels (c,d) are the obtained attenuation tomography results. New low attenuation areas L5 and L6 are marked.

Acknowledgements This work was funded by SISMO-VOL(CGL2014-57345) Spanish project, MED-SUV (EC-FP7 MEDiterranean SUpersite Volcanoes) European project and granted by Grupo de Investigación en Geofísica y Sismología from the Andalusian Regional Program. Edoardo Del Pezzo was partially granted by V2-Precursori project from DPC-INGV.

References

Abdel-Monen A, Watkins ND, Gast P (1972) Potassium-argon ages, volcanic stratigraphy and geomagnetic polarity history of the Canary Islands: Tenerife, La Palma and El Hierro. American Journal of Science 272:805–825

Ablay G (1997) Evolution of the Teide-Pico Viejo complex and magma system, Tenerife, Canary Islands. PhD thesis, University of Bristol

Ablay G, Kearey P (2000) Gravity constraints on the structure and volcanic evolution of Tenerife, Canary Islands. Journal of Geophysical Research 105:5783–5796

Almendros J, Ibáñez J, Alguacil G, Morales J, Del Pezzo E, La Rocca M, Ortiz R, Araña V, Blanco MJ (2000) A double seismic antenna experiment at Teide volcano: existence of local seismicity and lack of evidences of volcanic tremor. Journal of Volcanology and Geothermal Research 103:439–462

Almendros J, Ibáñez J, Carmona E, Zandomeneghi D (2007) Array analyses of volcanic earthquake and tremor recorded at Las Cañadas caldera (Tenerife Island, Spain) during the 2004 seismic activation of Teide volcano. Journal of Volcanology and Geothermal Research 160:285–299

Alparone S, Barberi G, Cocina O, Giampiccolo E, Musumeci C, Patané D (2012) Intrusive mechanism of the 2008-2009 Mt. Etna eruption: Constraints by tomographic images and stress tensor analysis. Journal of Volcanology and Geothermal Research 229-230:50–63

Ancochea E, Fúster JM, Ibarrola E, Cendrero A, Coello J, Hernan F, Cantagrel J, Jamond C (1990) Volcanic evolution of the Island of Tenerife (Canary Islands) in the ligth of new K-Ar data. Journal of Volcanology and Geothermal Research 44:231–249

Andújar J, Costa F, Martí J (2010) Magma storage conditions of the last eruption of Teide volcano (Canary Islands, Spain). Bulletin of Volcanology 72(4):381–395

Araña V (1971) Litología y estructura del edificio Cañadas, Tenerife (Islas Canarias). Estudios Geológicos 27:95–137

Blanco-Montenegro I, Nicolosi I, Pignatelli A, García A, Chiappini M (2011) New evidence about the structure and growth of ocean island volcanoes from aeromagnetic data: The case of Tenerife, Canary Islands. Journal of Geophysical Research 116

Bosshard E, MacFarlane DJ (1970) Crustal structure of the western Canary Island from seismic refraction and gravity data. Journal of Geophysical Research 75(26):4901–4918

Carracedo JC, Rodríguez-Bardiola E, Guillou H, Paterne M, Scaillet S, Pérez-Torrado FJ, Paris R, Fra-Paleo U, Hansen A (2007) Eruptive and structural history of Teide volcano and rift zone of Tenerife, Canary islands. Geological Society of America Bulletin 119:1027–1051

Coppo N, Schnegg PA, Heise W, Falco P, Costa R (2008) Multiple caldera collapses inferred from the shallow electrical resistivity signature of the Las Cañadas caldera, Tenerife, Canary Islands. Journal of Volcanology and Geothermal Research 170:153–166

Coppo N, Schnegg PA, Falco P, Costa R (2010) Conductive structures around Las Cañadas caldera, Tenerife (Canary Islands, spain): A structural control. Geologica Acta 8:67–82

Dañobeitia JJ, Canales JP (2000) Magmatic underplating in the Canary Archipelago. Journal of Volcanology and Geothermal Research 103(1):27–41

Dash BP, Bosshard E (1969) Seismic and gravity investigations around the western Canary Islands. Earth and Planetary Science Letters 7(2):169–177

De Barros L, Martini F, Bean CJ, García-Yeguas A, Ibáñez J (2012) Imaging magma storage below Teide volcano (Tenerife) using scattered seismic wavefields. Geophysical Journal International 191:695–706

De Gori P, Chiarabba C, Patané D (2005) Qp structure of mount etna: constraints for the physics of the plumbing system. Journal of Geophysical Research 110

De Lorenzo S, Gasparini P, Mongelli F, Zollo A (2001) Thermal state of the Campi Flegrei caldera inferred from seismic attenuation tomography. Journal of Geodynamics 32:467–486

De Siena L, Del Pezzo E, Bianco F, Tramelli A (2009) Multiple resolution seismic attenuation imaging at Mt. Vesuvius. Physics of the Earth and Planetary Interiors 173:17–32

De Siena L, Del Pezzo E, Bianco F (2010) Seismic attenuation imaging of Campi Flegrei: Evidence of gas reservoirs, hydrothermal basins and feeding systems. Journal of Geophysical Research 115

De Siena L, Waite G, Moran S, Thomas C (2013) Joint scattering and attenuation imaging of Mount Saint Helens reveals the melt paths feeding an erupting volcano. Submitted to Nature Geosciences

De Siena L, Thomas C, Aster R (2014) Multi-scale reasonable attenuation tomography analysis (MuRAT): an imaging algorithm designed for volcanic regions. Journal of Volcanology and Geothermal Research 277:22–35

Del Pezzo E (2008) Seismic wave scattering in volcanoes. Advances in Geophysics 50:353–371

Del Pezzo E, La Rocca M, Ibáñez J (1997) Observations of high-frequency scattered waves using dense array at Teide volcano. Bulletin of Seismological Society of America 87:1637–1647

Del Pezzo E, Bianco F, De Siena L, Zollo A (2006) Small scale shallow attenuation structure at Mt. Vesuvius, Italy. Physics of the Earth and Planetary Interiors 157:257–268

Domínguez Cerdeña I, Del Fresno C, Rivera L (2011) New insight on the increasing seismicity during Tenerife's 2004 volcanic reactivation. Journal of Volcanology and Geothermal Research 206:15–29

Eberhart-Phillips D, Reyners M, Chadwick M, Chiu JM (2005) Crustal heterogeneity and subduction processes: 3-d vp, vp/vs and q in the southern north island, new zealand. Geophysical Journal International 162:270–288

Fullea J, Camacho AG, Negredo AM, Fernndez J (2015) The Canary Islands hot spot: New insights from 3D coupled geophysical-petrological modelling of the lithosphere and uppermost mantle. Earth and Planetary Science Letters 409

Fúster JM, Araña V, Brandle JL, Navarro JM, Alonso V, Aparicio A (1968) Geología y volcanología de las Islas Canarias: Tenerife. Instituto Mallada, CSIC, 218 p

García O, Guzmán S, Martí J (2014) Stratigraphic correlation of Holocene phonolitic explosive episodes of the Teide-Pico Viejo Volcanic Complex, Tenerife. Journal of Geological Society 171:375–387

García-Yeguas A, Koulakov I, Ibáñez J, Rietbrock A (2012) High resolution P wave velocity structure beneath Tenerife Island (Canary Islands, Spain). Geophysical Journal International 117:doi: 10.1029/2011JB008,970.

Geyer A, Martí J (2010) The distribution of basaltic volcanism on Tenerife, Canary Islands: Implications on the origin and dynamics of the rift systems. Tectonophysics 483(3):310–326

Gottsmann J, Camacho AG, Martí J, Wooler L, Fernández J, García A, Rymer H (2008) Shallow structure beneath the Central Volcanic Complex of Tenerife from new gravity data: implications for its evolution and necent reactivation. Physics of the Earth and Planetary Interiors 168:212–230

Gudmundsson O, Finlayson DM, Itikarai I, Nishimura Y, Johnson W (2004) Seismic attenuation at rabaul volcano, papua new guinea. Journal of Volcanology and Geothermal Research 130:77–92

Hansen S, Thurber CH, Mandernach M, Haslinger F, Doran C (2004) Seismic Velocity and Attenuation Structure of the East Rift Zone and South Flank of Kilauea Volcano, Hawaii. Bulletin of the Seismological Society of America 94:1430–1440

Ibáñez J, Rietbrock A, García-Yeguas A (2008) Imaging an active volcano edifice at Tenerife Island, Spain. EOS Trans Am Geophys Un 89:289–300

Iribarren I (2014) Modelos geológicos en 3D de la isla de Tenerife. PhD thesis, University of Barcelona p 234 pp (in spanish)

Koulakov I (2009) Code ATOM-3D for 3D tomographic inversion based on active refraction seismic data

La Rocca M, Del Pezzo E, Simini M, Scarpa R, De Luca G (2001) Array analysis of seismograms for explosive sources: evidence for surface waves scattered at the main topographical features. Bulletin of the Seismological Society of America 91:219–231

Lodge A, Nippress S, Rietbrock A, García-Yeguas A, Ibáñez J (2012) Evidence for magmatic underplating and partial melt beneath the Canary Islands derived using teleseismic receiver functions. Physics of the Earth and Planetary Interior 212-213:44–54

Mantovani E, Viti M, Babbucci D, Albarello D (2007) Nubia-Eurasia kinematics: an alternative interpretation from Mediterranean and North Atlantic evidence. Annals of Geophysics 50(3)

Martí J, Gudmundsson A (2000) The Las Cañadas caldera (Tenerife, Canary Islands): an overlapping collapse caldera generated by magma-chamber migration. Journal of Volcanology and Geothermal Research 103:161–173

Martí J, Mitjavila J, Araña V (1994) Stratigraphy, structure and geochronology of the Las Caadas caldera (Tenerife, Canary Islands). Geological Magazine 131:715–727

Martí J, Ablay G, Bryan S (1996) Comment on "The Canary Islands: an example of structural control on the growth of large oceanic-island volcanoes" by J. C. Carracedo. Journal of Volcanology and Geothermal Research 72(1):143–149

Martí J, Hurlimann M, Ablay G, Gudmundsson A (1997) Vertical and lateral collapses on Tenerife (Canary Islands) and other volcanic ocean islands. Geology 25:879–882

Martí J, Geyer A, Andujar J, Teixó F, Costa F (2008) Assesing the potential for future explosive activity from Teide-Pico Viejo stratovolcanoes (Tenerife, Canary Islands). Journal of Volcanology and Geothermal Research 178:529–542

Martí J, Sobradelo R, Felpeto A, García O (2012) Eruptive scenarios of phonolitic volcanism at Teide-Pico Viejo volcanic complex (Tenerife, Canary Islandas). Bulletin of Volcanology 74:767–782

Martínez-Arevalo C, Patané D, Rietbrock A, Ibáñez J (2005) The intrusive process leading to the Mt. Etna 2001 flank eruption: Constraints from 3D attenuation tomography. Geophysical Research Letters 32:L21,309

Mezcua J, Buforn E, Udías A, Rueda J (1992) Seismotectonics of the Canary Islands. Tectonophysics 208:447–452

Morozov IB (2011) Mechanisms of geometrical seismic attenuation. Annals of Geophysics 54(3)

Neumann ER, Wulff-Pedersen E, Simonsen S, Pearson NJ, O'Reilly SY, Martí J, Mitjavila J (1999) Evidence for fractional crystalization of periodically refilled magma chambers in Tenerife, Canary Islands. Journal of Petrology 40:1089–1123

Ohlendorf SJ, Thurber C, Pesicek JD, Prejean SG (2014) Seismicity and seismic structure at Okmok Volcano, Alaska. Journal of Volcanology and Geothermal Research 278:103–119

Piña-Varas P, Ledo J, Queralt P, Marcuello A, Bellmunt F, Hidalgo R, Messeiller M (2014) 3-D Magnetotelluric Exploration of Tenerife Geothermal System (Canary Islands, Spain). Surveys in Geophysics 35:1045:1064

Pittari A, Cas RAF, Wolff JA, Nichols HJ, Larson PB, Martí J (2008) The use of lithic clast distributions in pyroclastic deposits to understand pre-and syn-caldera collapse processes: A case study of the Abrigo Ignimbrite, Tenerife, Canary Islands. Developments in Volcanology 10:97–142

Pous J, Schnegg PA, Muoz G, Martí J, Soriano C (2002) Magnetotelluric study of the Las Cañadas caldera (Tenerife, Canary Islands): structural and hydrogeological implications. Earth and Planetary Science Letters 204:249–263

Prudencio J, Del Pezzo E, García-Yeguas A, Ibáñez J (2013a) Spatial distribution of intrinsic and scattering seismic attenuation in active volcanic islands, I: model and the case of Tenerife Island. Geophysical Journal International 195 (3):1942–1956, doi: 10.1093/gji/ggt361

Prudencio J, Ibáñez J, García-Yeguas A, Del Pezzo E (2013b) Spatial distribution of intrinsic and scattering seismic attenuation in active volcanic islands, II: Deception island images. Geophysical Journal International 195 (3):1957–1969, doi: 10.1093/gji/ggt360

Prudencio J, De Siena L, Ibáñez J, Del Pezzo E, García-Yeguas A, Díaz-Moreno A (2015) The 3D attenuation structure of Deception Island (Antarctica). Surveys in Geophysics DOI: 10.1007/s10712-015-9322-6

Roest WR, Dañobeitia JJ, Verhoef J, Collette BJ (1992) Magnetic anomalies in the Canary Basin and the Mesozoic evolution of the central North Atlantic. Marine Geophysical Researchers 14:1–24

Romero-Ruiz C (1991) Las manifestaciones volcánicas históricas del archipiélago canario. Consejería Territorial Gobierno Autónomo de Canarias, Santa Cruz de Tenerife, España p pp. 1463

Sato H, Fehler M, Maeda T (2012) Seismic wave propagation and scattering in heterogeneous Earth. 2nd edition, Springer-Verlag Berlin Heidelberg

Schurr B, Asch G, Rietbrock A, Trumbull R, Haberland CH (2003) Complex patterns of fluid and melt transport in the central Andean subduction zone revealed by attenuation tomography. Earth and Planetary Science Letters 215:105–119

Soler-Javaloyes V, Carracedo JC (2013) Geophysical Investigations of the Teide Volcanic Complex. Springer, Berlin, Heidelberg

Thrilwall M, Singer BS, Marriner GF (2000) 39Ar/40Ar ages and geochemistry of the shield stage of Tenerife, Canary Islands, Spain. Journal of Volcanology and Geothermal Research 103:247–297

Tramelli A, Del Pezzo E, Fehler M (2009) 3D scattering image of Mt. Vesuvius. Bulletin of Seismological Society of America 99:1962–1972

Vanorio T, Virieux J, Capuano P, Russo G (2005) Three-dimensional tomography from P wave and S wave microearthquake travel times and rock physics characterization of the Campi Flegrei Caldera. Journal of Geophysical Research 110(B03201):doi:10.129/2004JB003,102

Verhoef J, Collette BJ, Dañobeitia JJ, Roeser HA, Roest WR (1991) Magnetic anomalies off West-Africa (20-38 N). Marine Geophysical Researchers 13(2):81–103

Villasante-Marcos V, Finizola A, Abella R, Barde-Cabusson S, Blanco MJ, Brenes B, Cabrera V, Casas B, De Agustín P, Di Gangi F, Domínguez I, García O, Gomis A, Guzmán J, Iribarren I, Levieux G, López C, Luengo-Oroz N, Martín I, Moreno M, Meletlidis S, Morin J, Moure D, Pereda J, Ricci T, Romero E, Schutze C, Suski-Ricci B, Torres P, Trigo P (2014) Hydrothermal system of Central Tenerife Volcanic Complex, Canary Islands (Spain), inferred from self-potential measurements. Journal of Volcanology and Geothermal Research 272:59–77

Watts AB, Pierce C, Collier J, Dalwood R, Canales JP, Hens-Tock TJ (1997) A seismic study of lithosphere flexure in the vicinity of Tenerife, Canary Islands. Earth and Planetary Science Letters 146:431–447

Yoshimoto K, Sato H, Ohtake M (1993) Frequency-dependent attenuation of P and S waves in Kanto area, Japan, based on the coda-normalization method. Geophysical Journal International 114:165–174

Zandomeneghi D, Barclay A, Almendros J, Ibáñez J, Wilcock WSD (2009) Crustal structure of Deception Island volcano from P-wave seismic tomography: tectonic and volcanic implications. Journal of Geophysical Research 114

Table 1.

V_p	V_s	Q_p^{-1}	Q_s^{-1}	V_p/V_s	Interpretation
L	L	H	H	L	Fractured porous zone, typically on surface (e.g. Gudmundsson et al 2004)
H	?	H	?	?	Fractured zone with the presence os fluids (e.g. De Gori et al 2005)
L	L	H	H	A/H	Magma, fluids (e.g. Schurr et al 2003)
L	L	H	L	L/A	Presence of gasses (e.g. Hansen et al 2004)
H	H	L	L	A	Compact zone, tipically at high depth (e.g. Eberhart-Phillips et al 2005)
H	?	L	?	?	Volcanic conduit (e.g.De Gori et al 2005)

Figure 1
Click here to download Figure: Figure 1.png

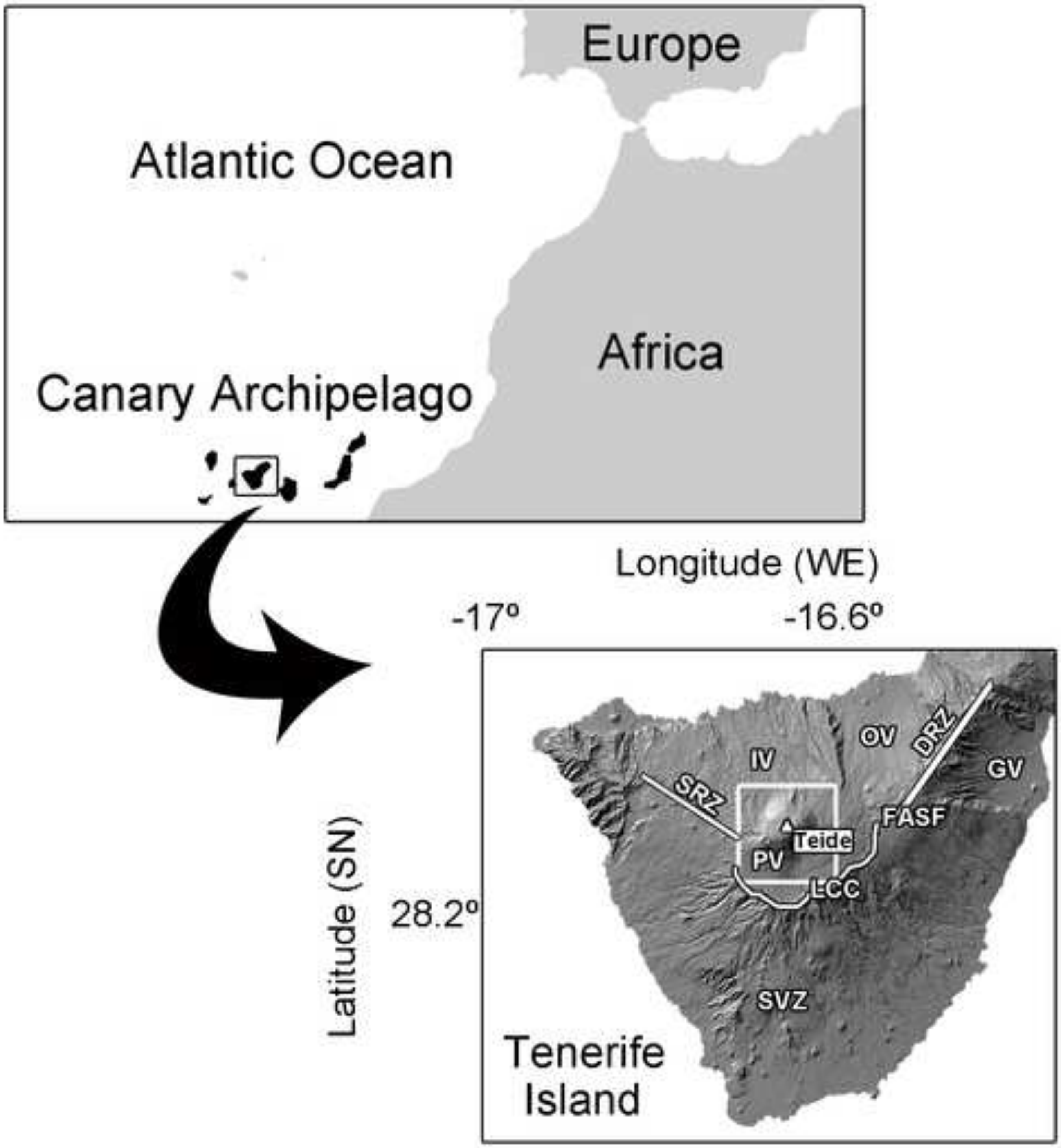

Figure 2
Click here to download Figure: Figure 2.png

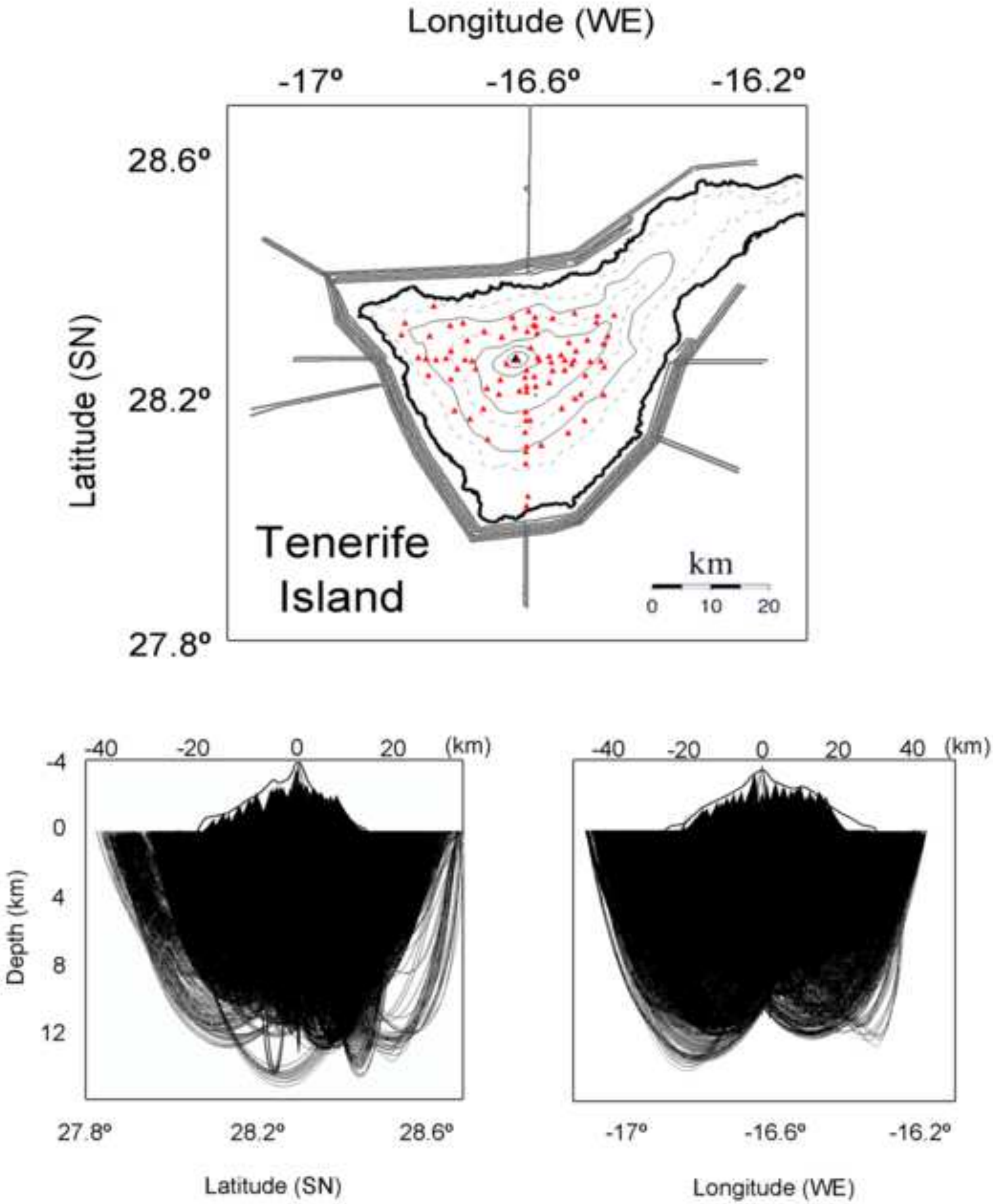

Figure 3
Click here to download Figure: Figure 3.png

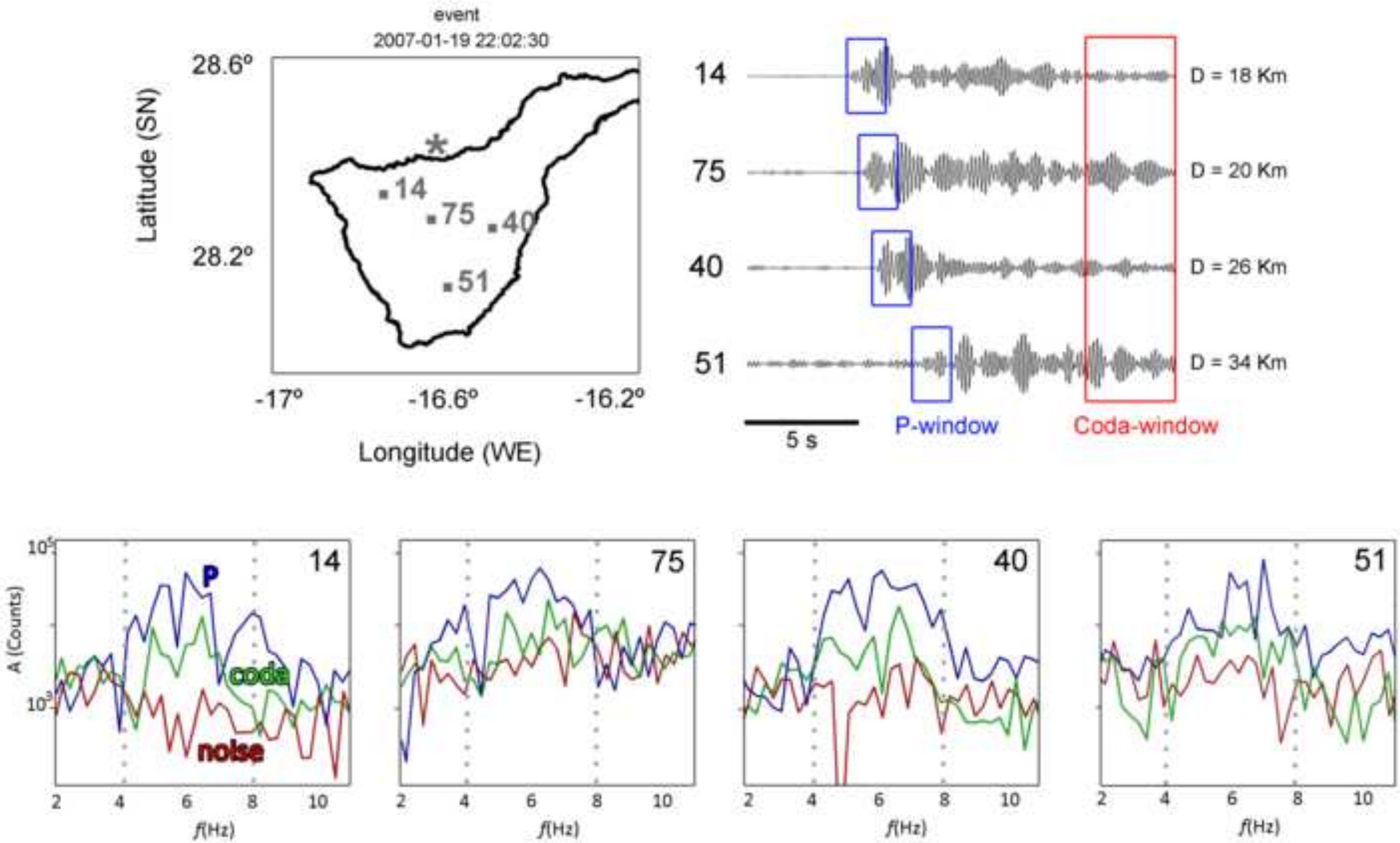

Figure 4
Click here to download Figure: Figure 4.png

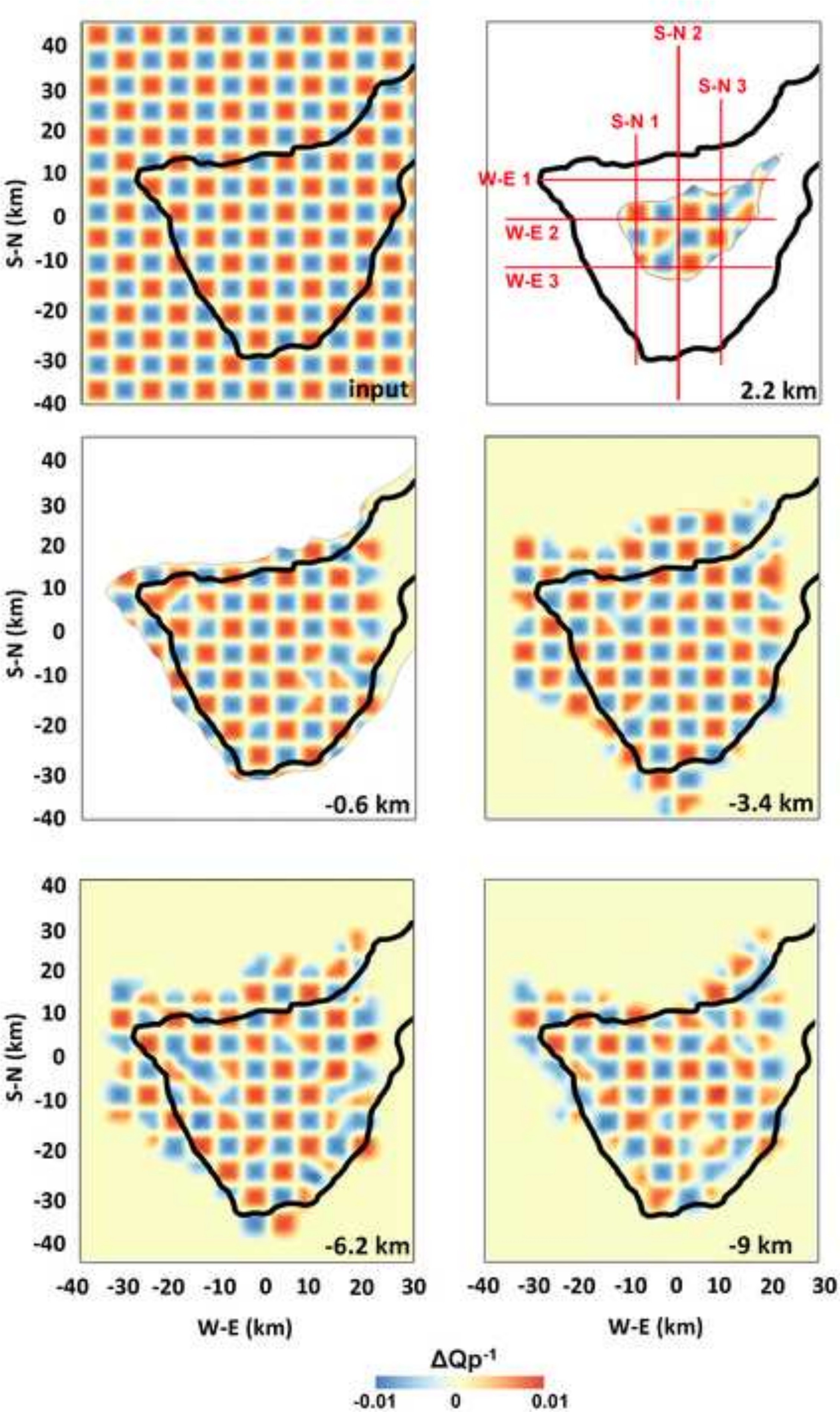

Figure 5

Click here to download Figure: Figure 5.png

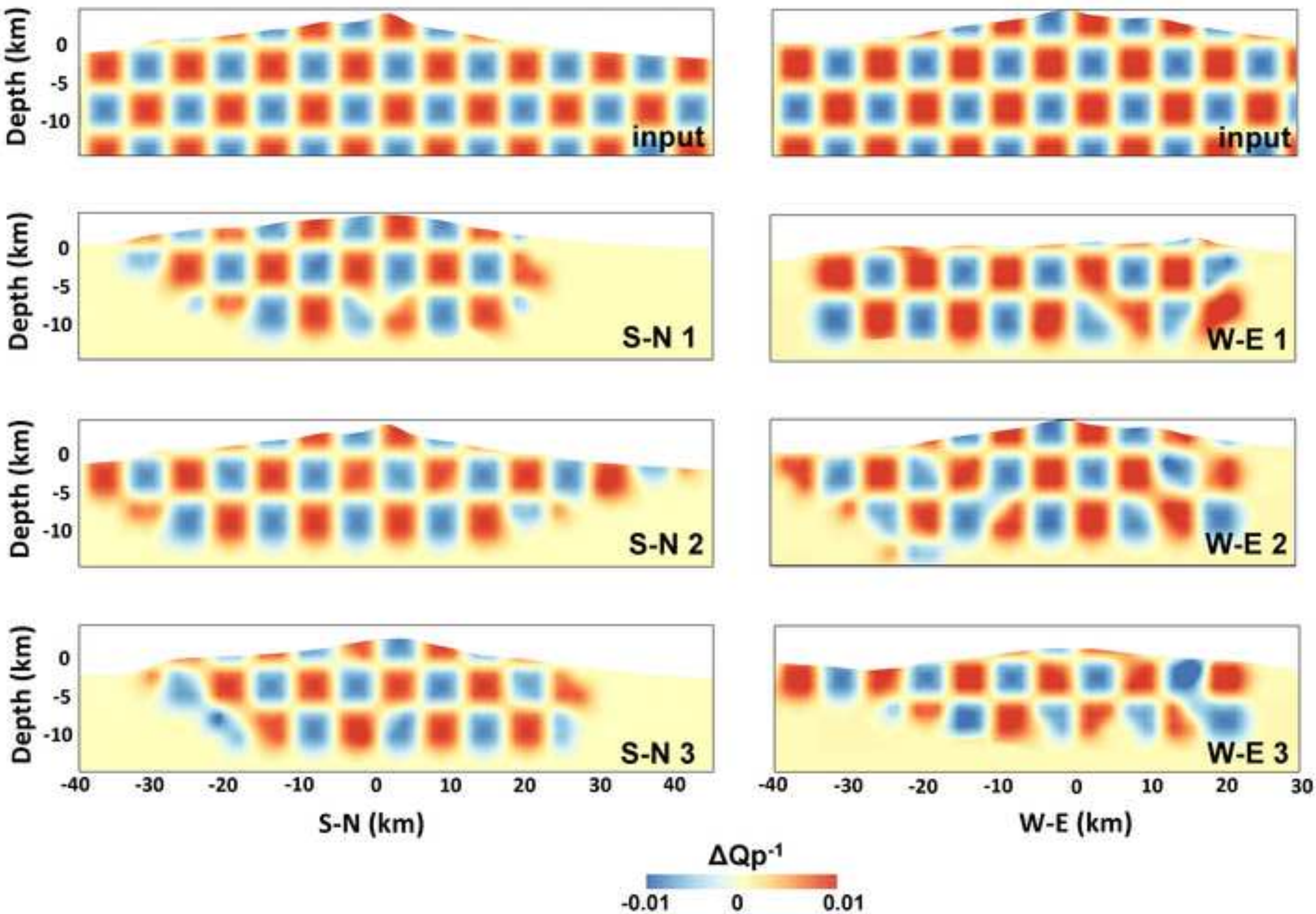

Figure 6
Click here to download Figure: Figure 6.png

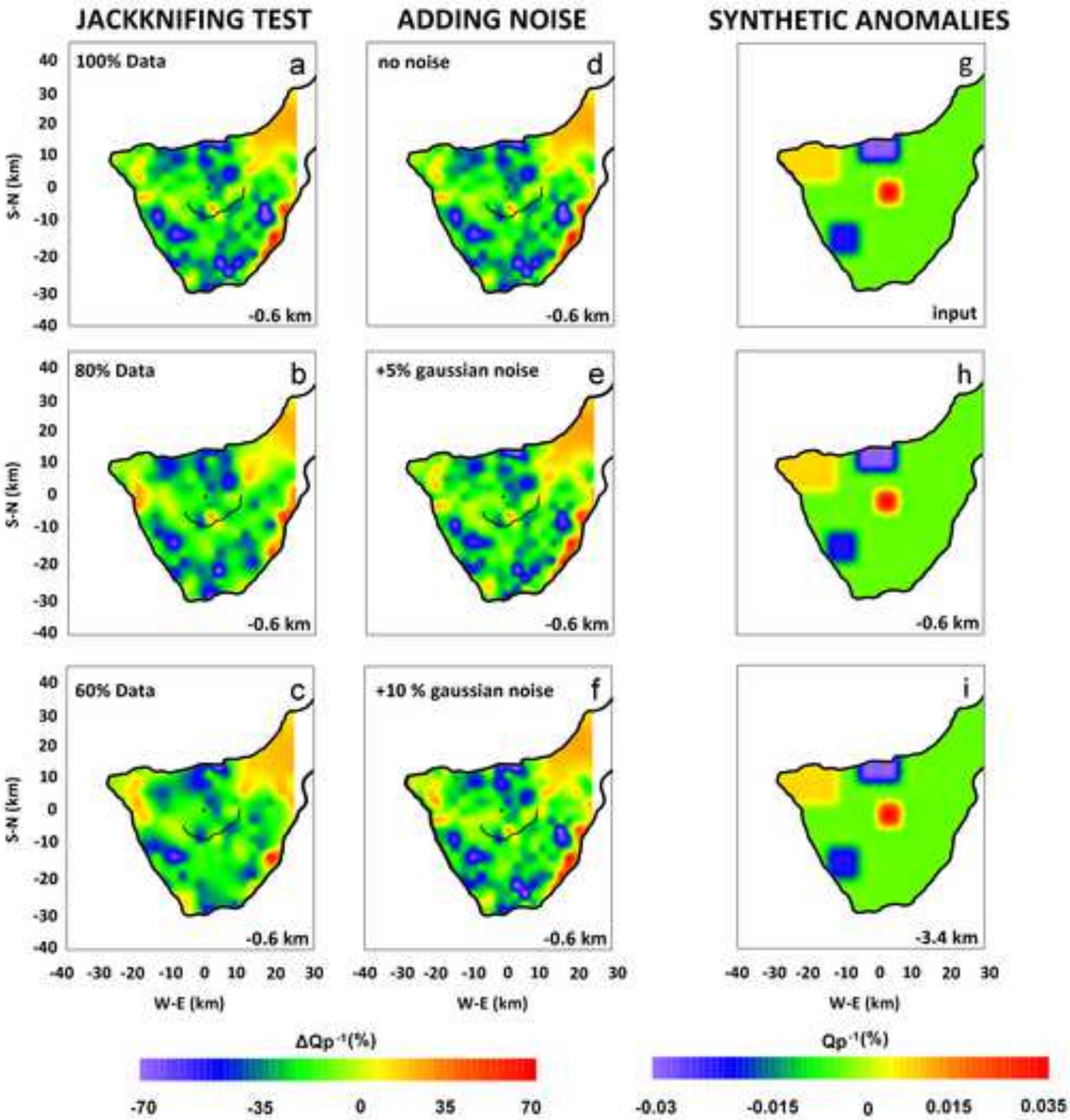

Figure 7
Click here to download Figure: Figure 7.png

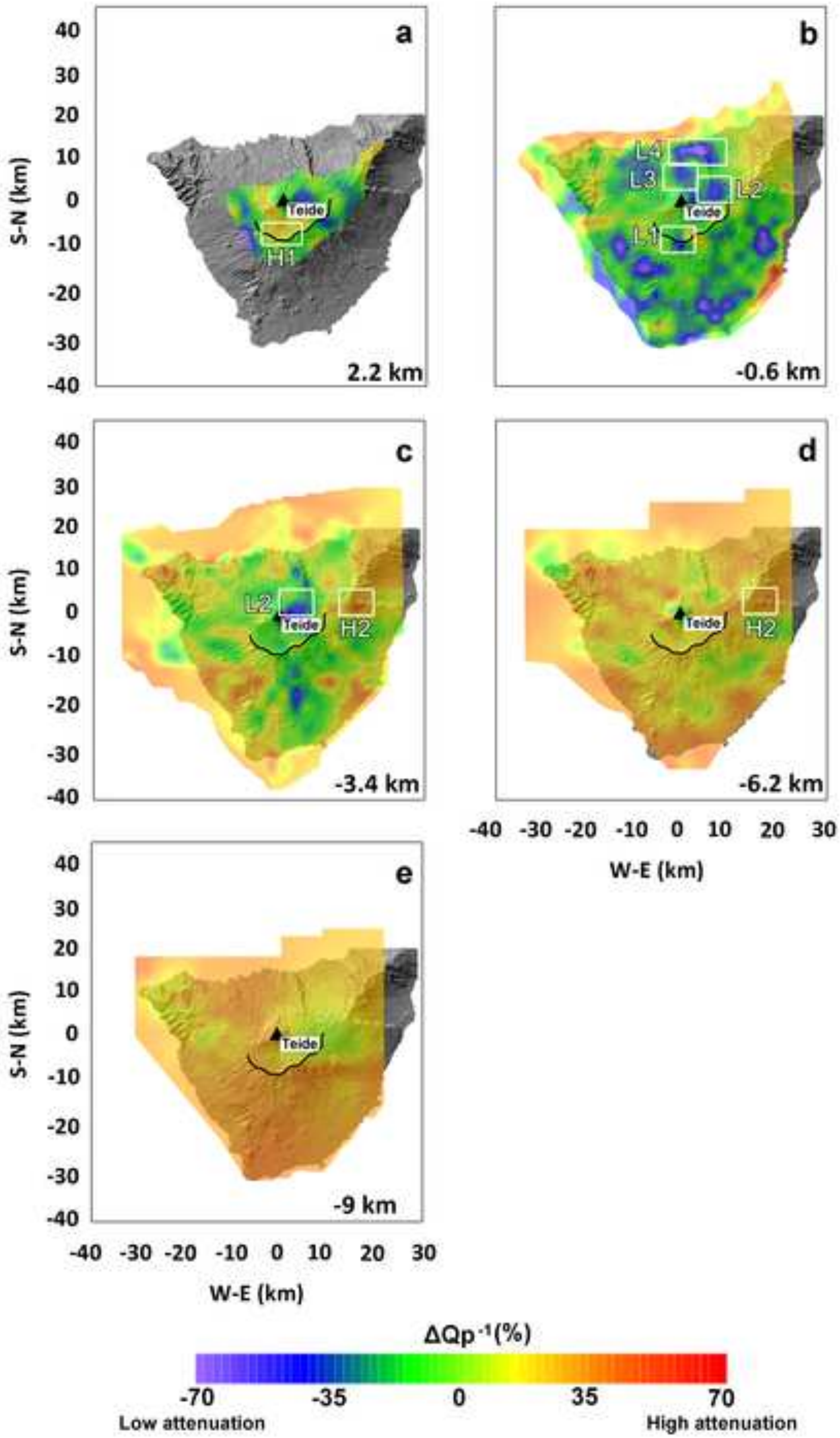

Figure 8
Click here to download Figure: Figure 8.png

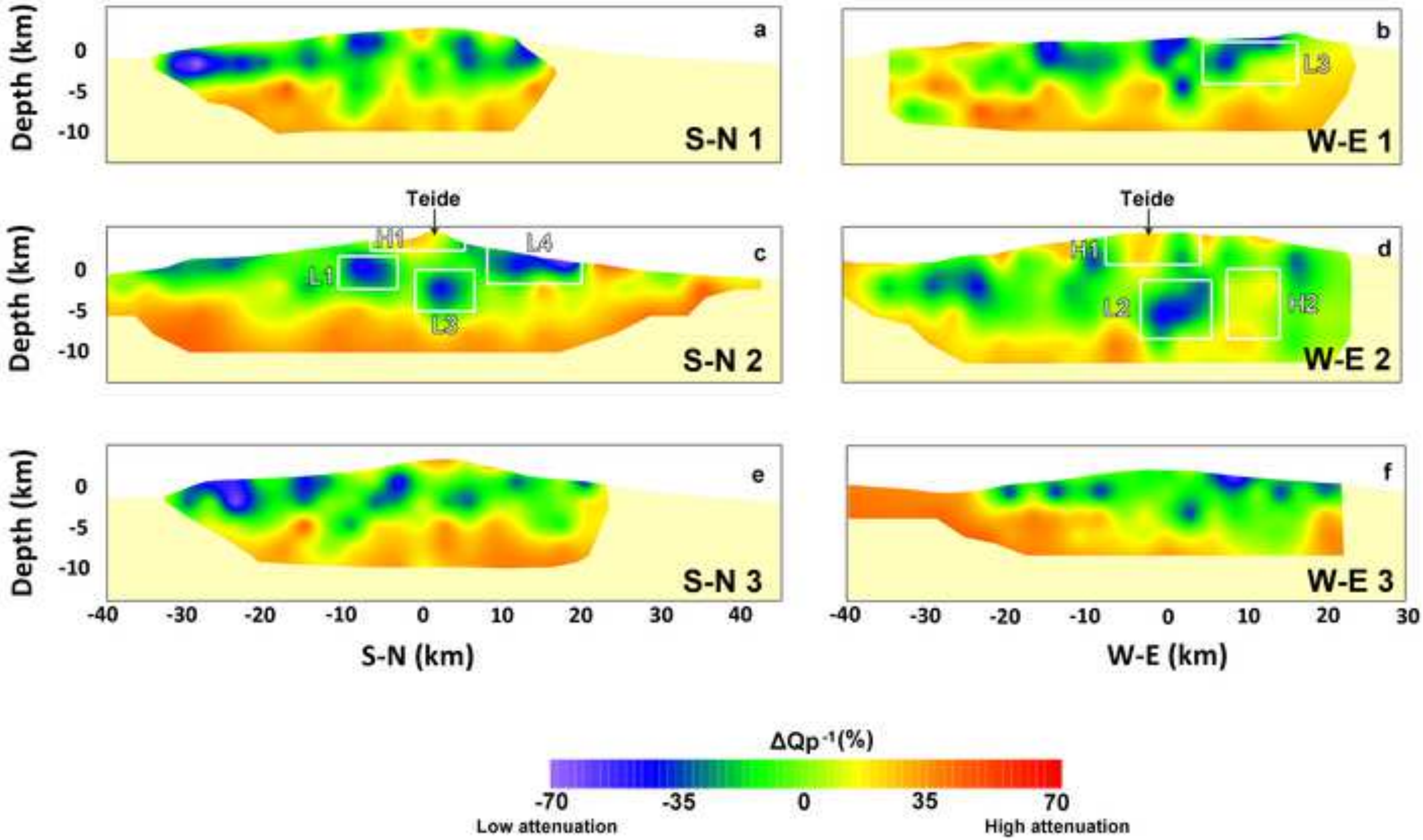

Figure 9
Click here to download Figure: Figure 9.png

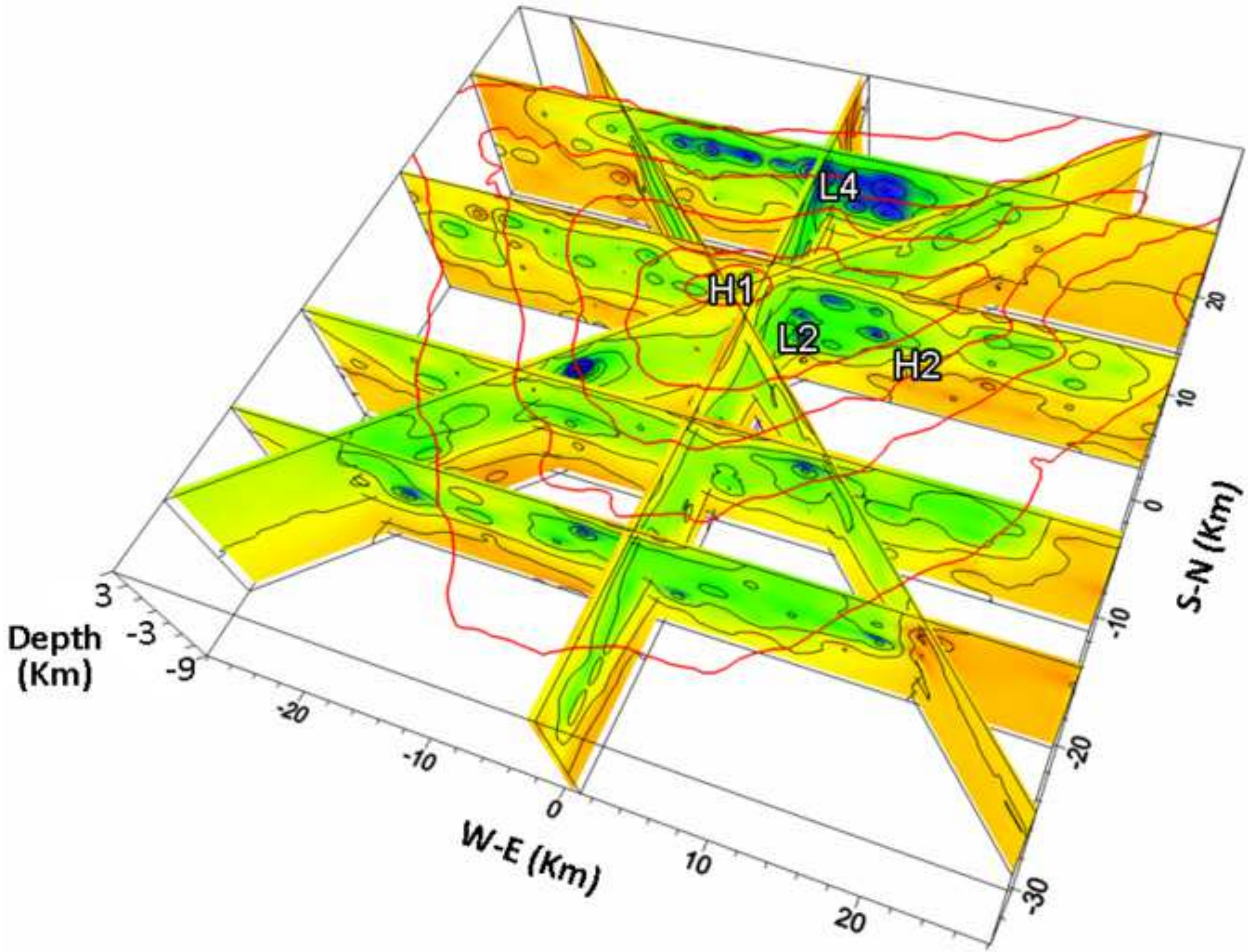

Figure 10

Click here to download Figure: Figure 10.png